RESEARCH PAPER

Detailed Investigation on Possible Phases during Solid-State Synthesis of MnAl Intermetallic Compound

Majid Tavoosi

* ma.tavoosi@gmail.com

Department of Materials Engineering, Malek-Ashtar University of Technology, Iran

Abstract: The present study focuses on the phase and structural features of the MnAl intermetallic compound during solid-state synthesis. In this regard, the milling process was done in different $Mn_{50+x}Al_{50-x}$ ($0< x< 7.5$) powder mixtures and the prepared samples were evaluated using X-ray diffractometer, scanning and transmission electron microscopy, differential thermal analysis and vibrating sample magnetometer. The results showed that the τ-MnAl magnetic phase with L10 structure could not be formed during the milling and low-temperature annealing. During the milling process, Al atoms dissolve in the Mn network and a single β-Mn supersaturated solid solution (SSSS) forms. The β-Mn (SSSS) phase is unstable and transforms into the icosahedral quasi-crystal as well as $γ_2$-Al_8Mn_5 and β-Mn stable phases during subsequent annealing.

Keywords: MnAl permanent magnet, Mechanical alloying, Icosahedral phase.

1. INTRODUCTION

Mn-Al alloys, due to favorable magnetic properties and low production cost, are considered a suitable alternative for rare-earth permanent magnets [1-3]. The magnetic features of these alloys can be correlated to the formation of τ-MnAl intermetallic compound with an ordered $L1_0$ structure. This phase, which was introduced by Kono in 1950, is the individual ferromagnetic segment in the Mn-Al system and can be formed in the composition range of 49-60 at. % of Mn. Based on the literature, the τ-MnAl compound only forms during controlled annealing of the as-quenched $ε$ -phase in a temperature range of 400-700°C. This phase is unstable and easily transforms into non-magnetic $γ_2(Al_8Mn_5)$ and β (Mn) phases during the production procedure. Due to the formation of the mentioned phases, the magnetization obtained in the case of the MnAl compound is much lower than its theoretical value (144 emu/g) [4-6].

To achieve the optimized magnetic properties in the MnAl compound, it is necessary to have a correct understanding of phase transformations in this system. In this regard, various researchers have tried to investigate the structure and phase changes in the MnAl compound by changing the synthesis method and adding different alloying elements. For instance, the consequence of Ni adding on magnetic and structural properties of the as-sputtered MnAl phase was evaluated by

Matsumoto et al. [7]. In this research, the optimal atomic percentage of Ni element for stabilizing the τ-MnAl phase has been recognized as about 3 at. %. Zeng et al. [8] also stated that adding carbon to τ-MnAl alloy has significant effects on increasing the saturation magnetization and decreasing the anisotropy field. It was reported that the ordered $L1_0$ structure of τ-MnAl is not stable and decomposes to non-magnetic $γ_2$ and β phases during the milling process. In this regard, Wang et al. [9] report on the effect of the Zn element on the stabilization of $L1_0$, Liu et al. [1] investigation about the steadiness and magnetic features of MnAl alloy in the presence of B and C and Manchanda et al. [10] study about the outcome of Fe adding on the magnetic features of MnAl alloy are also worth mentioning.

However, despite extensive studies about the synthesis methods and stabilization of the magnetic phase in the MnAl system [10-19], it seems that the non-equilibrium and quasi-stable phases in this alloying system have not yet been well evaluated. According to this point, the current research aimed to investigate the structural and phase changes in the $Mn_{50+x}Al_{50-x}$ ($0< x< 7.5$) system during the milling and annealing processes.

2. EXPERIMENTAL PROCEDURES

Powders of Al (Merck, d= 60 μm, purity of 99.8%) and manganese (Merck, d= 50 μm, purity

of 99.8%) were used as precursors in this research. Elemental powders with the formulation $Mn_{50+x}Al_{50-x}$ (0< x <7.5) were ground in a planetary ball mill (rotating speed of 300 rpm and a ball-to-powder ratio of 10:1). Annealing process was done at 500 and 750°C (based on DSC results). Before annealing, the powder samples were sealed in a quartz ampoule under a vacuum of 10^{-3} pa to prevent oxidation during annealing. XRD test was done using an X-ray diffractometer (Asan ware model) with Cu K_{α} radiation and step size of 0.05°. The microstructural characteristics and shape of the samples were analyzed using a scanning electron microscope (Mira 3-XMU) and a transmission electron microscope (Jeol-JEM-3010). Also, differential scanning calorimetry (DSC) was performed to check the thermal stability of alloys using DTA L81/1750. The samples were placed in alumina containers and heated in an argon atmosphere to a temperature of 1300°C with a rate of 20°C/min. The magnetic properties of the alloys were also measured using a vibrating sample magnetometer (VSM) at room temperature.

3. RESULTS AND DISCUSSION

To explore the consequence of the milling procedure on the structural characteristics of different $Mn_{50+x}Al_{50-x}$ (0< x< 7.5) compounds, powder samples were milled at different times and the prepared specimens were evaluated utilizing the XRD technique. For instance, the X-ray diffraction patterns related to the $Mn_{50}Al_{50}$ powder mixture after performing the milling process at different times up to 20 h are accessible in Fig. 1. As can be realized, the diffraction patterns of the milled powders at the initial stage of milling include the peaks related to α-Mn, β-Mn and Al phases. By continuing the milling process for longer times, the intensity of the peaks related to Al gradually decreases and completely vanishes after 20 h. In this case, the corresponding peaks to α-Mn are shifted towards the lower degrees.

The gradual removal of Al peaks and the displacement of α-Mn peaks indicate the dissolution of Al atoms (184 pm) into the Mn network (140 pm) and the formation of a single β-Mn supersaturated solid solution (SSSS). The formation of a solid solution during the mechanical alloying process is due to the large amount of lattice strain energy which is absorbed

by the milled powders. These strains are capable of providing a driving force for creating many vacancies in the lattice of the milled powder so that the activation energy of the alloying elements decreases and gives rise to an increase in diffusivity [20, 21]. Thereby the alloying elements tend to migrate to the lattice defects and consequently solid solution forms. The SEM micrographs of $Mn_{50}Al_{50}$ powder mixture after 20 h of milling process are presented in Fig. 2. As seen, the shape of the particles is unequal and angular with a mean size of ~23 μm. Accordingly, the structural changes of $Mn_{50+x}Al_{50-x}$ (0< x< 7.5) of the powder mixture during the grinding process (up to 20 hours) can be written as follows:

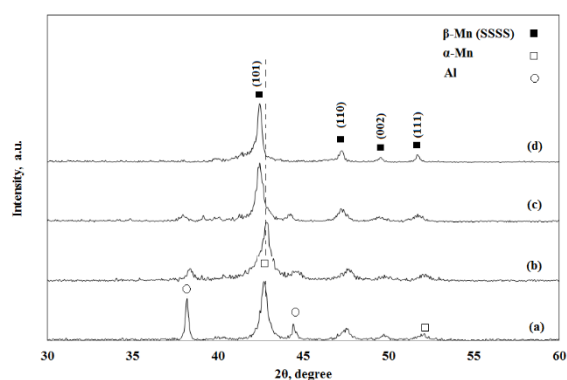Powder mixture→ α-Mn + β-Mn→ β-Mn (SSSS)

Fig. 1. The X-ray diffraction patterns of $Mn_{50}Al_{50}$ powder mixture after various milling times; a) 5, b) 10, c) 15 and d) 20 h.

Based on Fig. 1 (d), four diffraction peaks with (101), (110), (002) and (111) indices have appeared in the diffraction pattern related to the β-Mn (SSSS) phase. These peaks are very similar to the τ-MnAl phase-related peaks. Of course, due to the lack of peaks with (100) and (001) indices, this is not an order $L1_0$ structure. The $L1_0$ structure (space group P4/mm), determined by the high uniaxial crystal magnetic anisotropy, consists of alternating layers of two different elements, parallel to the tetragonal c-axis, forming a natural superlattice. The quadrilateral distortion of this phase along the c-axis is the reason for the crystalline magnetic anisotropy of the system. The value of this anisotropy is usually in the range of K1~106-107 J/m^3. In this structure, Mn atoms occupy (0, 0, 0) positions while Al atoms occupy (1/2, 1/2, 1/2) positions. Each crystallite site in the $L1_0$ structure has a different probability of being occupied by two types of atoms.
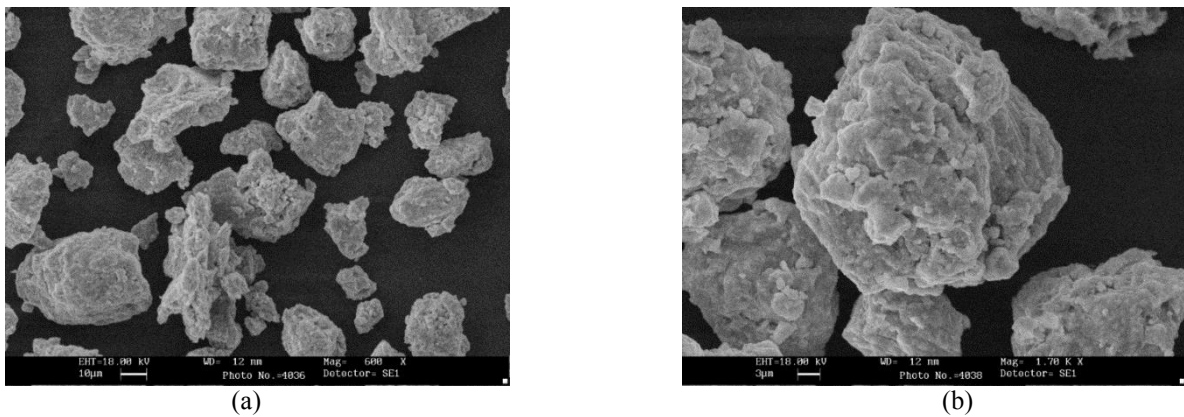
2

(a)   (b)

Fig. 2. The SEM micrographs of Mn$_{50}$Al$_{50}$ alloy after 20 h of milling process (at two different magnifications).

During milling or other non-equilibrium processes, this regular chemical structure can be transformed into a disordered face-centred cubic (β-Mn) structure through order-disorder transformation. In this structure, the occupation of a specific atomic site by each of the two constituent elements is equal. This order-disorder transition leads to a change in the magnetic properties of MnAl from ferromagnetic to paramagnetic. This issue can be well proven by considering the magnetic hysteresis loops of

different milled Mn$_{50+x}$Al$_{50-x}$ (0< x< 7.5) samples in Fig. 3. As seen, none of the samples has ferromagnetic properties after the milling process. This outcome is consistent with Lucis [15], Jian [16] and Lu et al. [17] about the disordering of the τ-MnAl phase during the milling process.

In this regard, the DSC heating trace of Mn$_{50}$Al$_{50}$ alloy after a milling time of 20 h is exhibited in Fig. 4. As can be observed, this graph contains one exothermic and one endothermic peak.
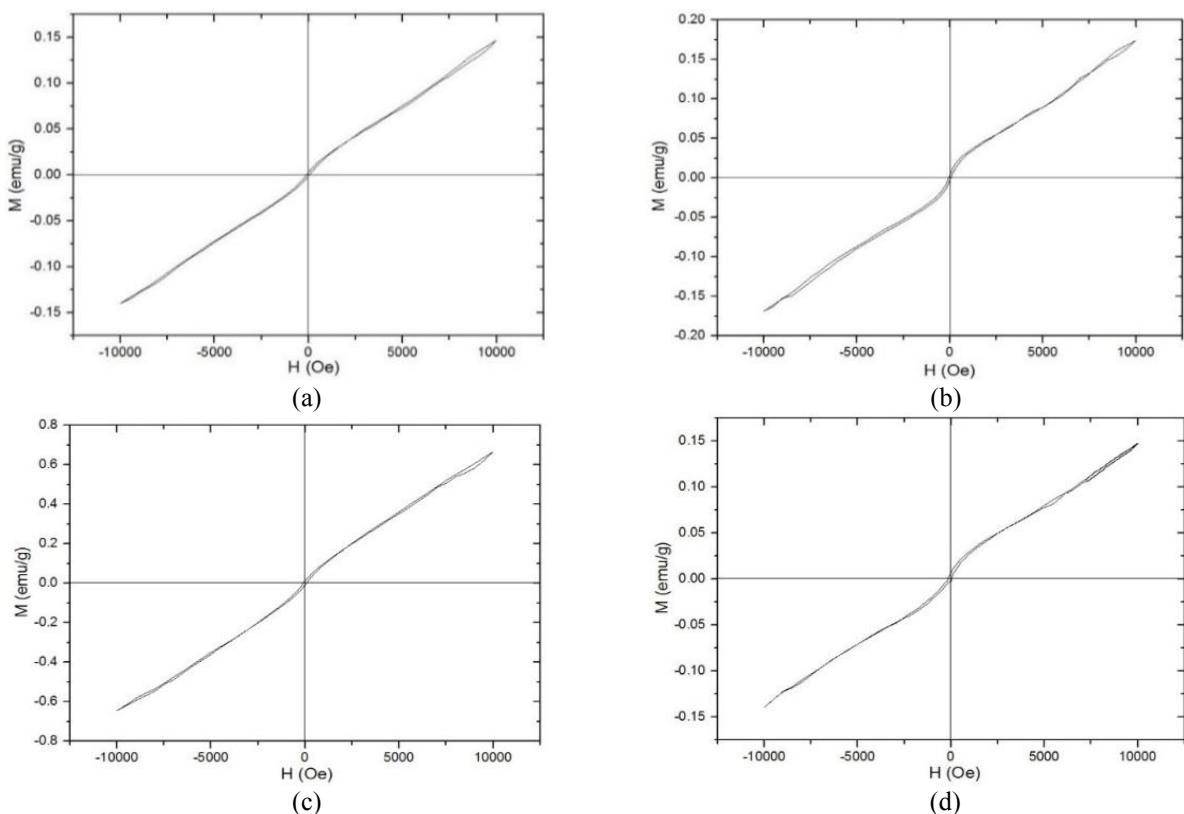

(a)   (b)

(c)   (d)

Fig. 3. VSM hysteresis loops of different Mn$_{50+x}$Al$_{50-x}$ alloy after 20 h of milling process with different amounts of Al content (x); a) 0, b) 2.5, c) 5 and d) 7.5.

3

The endothermic peak around 1293°C is correlated to the melting of the $Mn_{50}Al_{50}$ compound. To investigate the possible phase transformations in the $Mn_{50}Al_{50}$ powder mixture before the exothermic peak in Fig. 4 (around 680°C), the annealing process was performed at 500°C for 90 and 180 min.
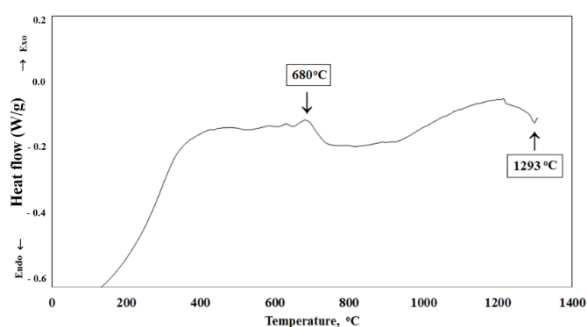

Fig. 4. The DSC heating trace of $Mn_{50}Al_{50}$ alloy after 20 h of milling time.

The diffraction patterns of the annealed samples are shown in Fig. 5. Based on this figure, the formed β-Mn (SSSS) phase is unstable and gradually transforms into the icosahedral quasi-crystalline phase during the low-temperature annealing process up to 180 min. To prove the creation of the aforementioned phase, the SEM and TEM micrographs of the annealed powder at 500°C for 180 min are presented in Figs. 6 and 7, respectively. The formation of powder particles with spherical morphology (close to the form of icosahedron deposits) in Fig. 6 and the electron diffraction pattern presented in Fig. 7 can prove the formation of an icosahedron phase in the structure.

The magnetic hysteresis loops of $Mn_{50+x}Al_{50-x}$ (0< x< 7.5) samples after the annealing process are accessible in Fig. 8. Based on this figure, during the low-temperature annealing process, the magnetic behavior changes from paramagnetism to weak ferromagnetism and the maximum magnetization value has reached to about 1.2 emu/g.
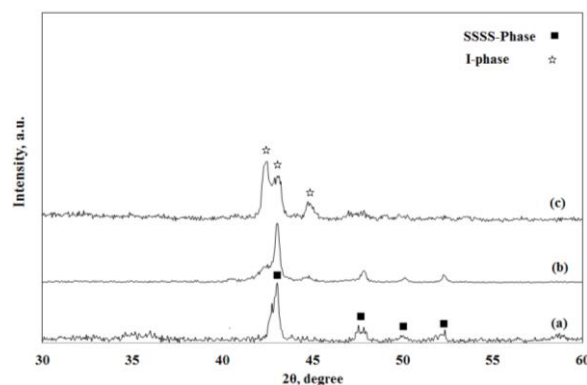

Fig. 5. The XRD patterns of $Mn_{50}Al_{50}$ milled sample after the annealing process at 500°C for a) 30, b) 90 and c) 180 min.

The icosahedral phase (I-phase) is paramagnetic and the weak ferromagnetic behavior of the annealed specimens can be related to the partial formation of the ordered $L1_0$ structure during annealing. However, the percentage of this phase is less than 5 vol.% which cannot be detected by X-ray diffractometry.

To inspect the phase and structural variations in the milled samples related to the DSC endothermic peak at 680°C (Fig. 4), the XRD patterns of $Mn_{50}Al_{50}$ alloy after the annealing step at 700°C for 90 and 180 min are exhibited in Fig. 9. As seen, during the annealing process, several peaks corresponding to Al_8Mn_5 phase (γ_2-phase) appear in XRD patterns.
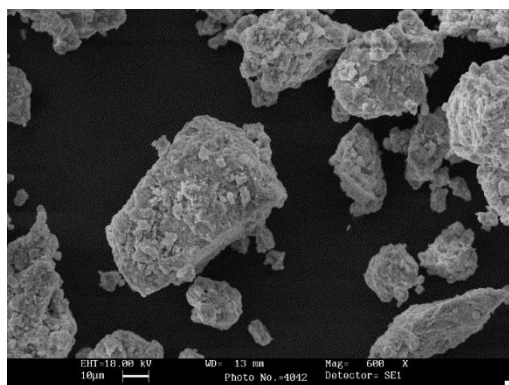
(a)
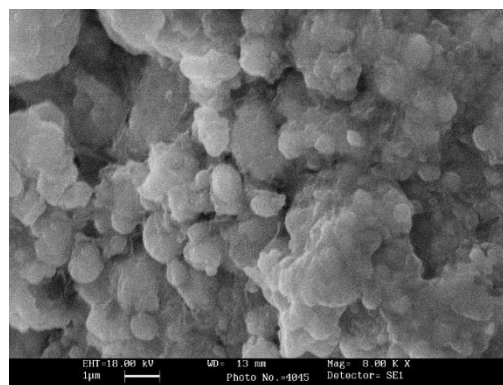
(b)

Fig. 6. The SEM micrographs of milled $Mn_{50}Al_{50}$ sample after annealing at 500°C for 180 min in two magnifications.
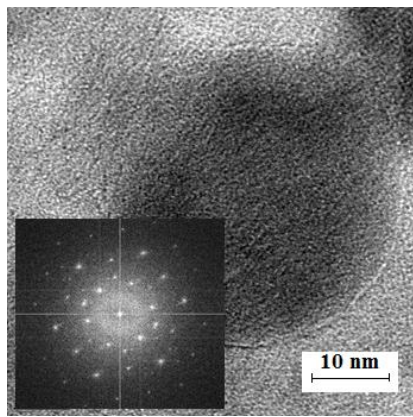
Fig. 7. The TEM image and EDP of milled $Mn_{50}Al_{50}$ alloy after annealing at 500°C for 180 min.

This point illustrates that the formed Icosahedral phase completely transforms into equilibrium β and γ_2 phases during annealing at higher temperatures. In this regard, the morphology of annealed alloys at 700°C is obtainable in Fig. 10. Compared to Fig. 6, the particle morphology completely changes to a semi-cubic morphology with a mean particle size of 1 μm. Due to the formation of non-magnetic β and γ_2-phases, the annealed samples at 700°C do not show proper magnetic properties. This point can be proven by attention to the magnetic hysteresis loops related to $Mn_{50+x}Al_{50-x}$ (0< x< 7.5) annealed samples at 700°C in Fig. 11.

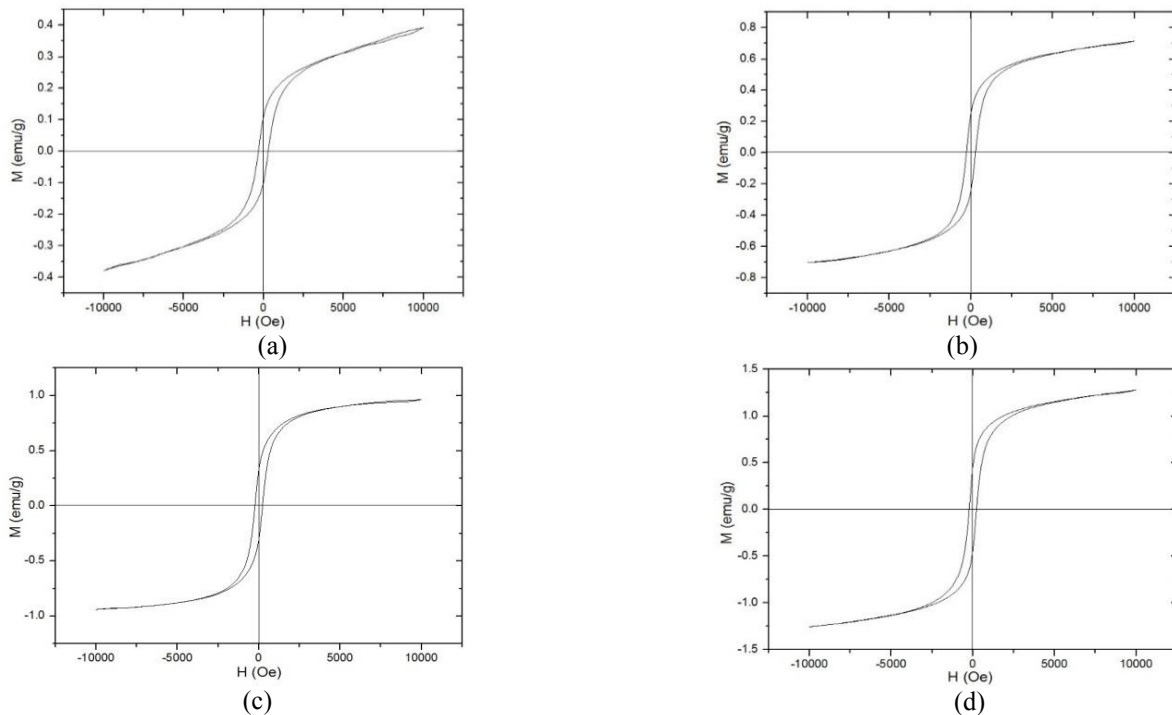**Fig. 8.** The VSM hysteresis loops of different $Mn_{50+x}Al_{50-x}$ powder mixtures after annealing at 500°C for 180 min; a) x= 0, b) x= 2.5, c) x= 5 and d) x= 7.5.
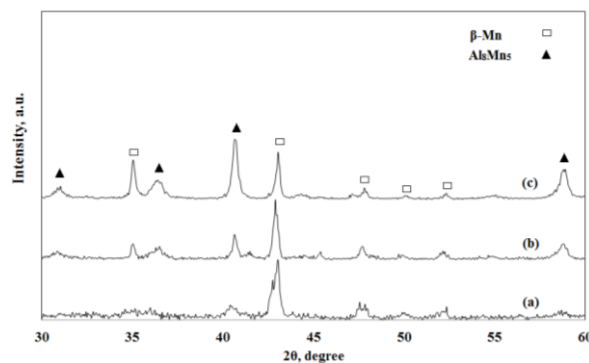

Fig. 9. The XRD patterns of the milled $Mn_{50}Al_{50}$ sample after the annealing process at 700°C for a) 30, b) 90 and c) 180 min.
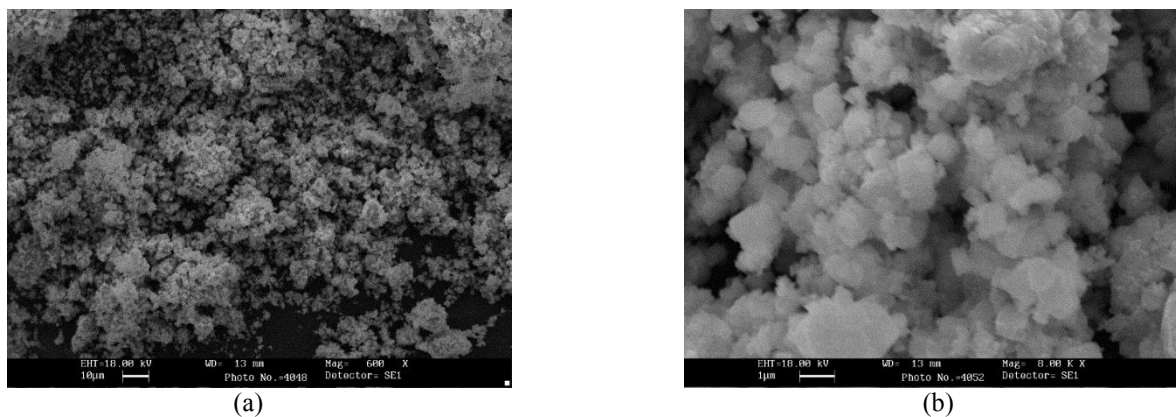
5

(a)

(b)

Fig. 10. The SEM micrographs of milled $Mn_{50}Al_{50}$ sample after annealing at 700°C for 180 min in two magnifications.
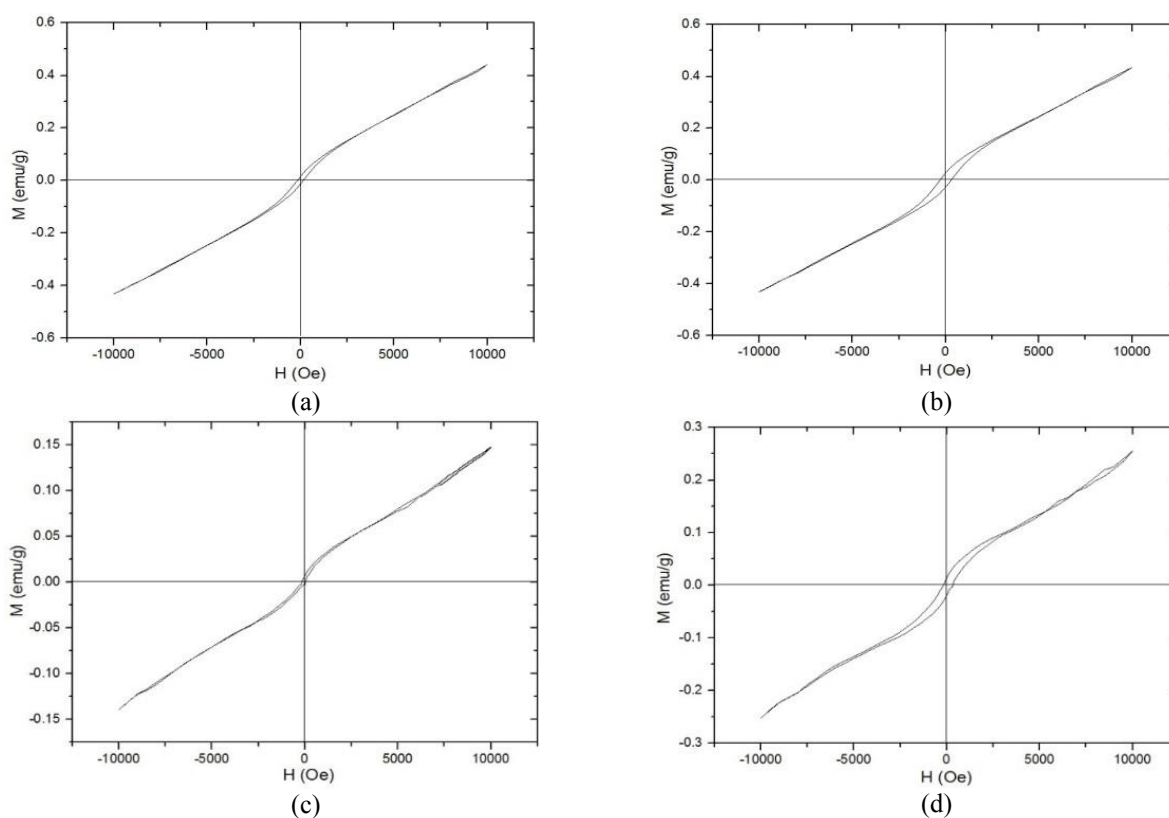

(a)

(b)

(c)

(d)

Fig. 11. The VSM hysteresis loops of different $Mn_{50+x}Al_{50-x}$ powder mixtures after annealing at 700°C for 180 min; a) x= 0, b) x= 2.5, c) x= 5 and d) x= 7.5.

4. CONCLUSIONS

From the investigation of structural and magnetic features of different $Mn_{50+x}Al_{50-x}$ (0< x< 7.5) alloys during the milling and annealing process, the following conclusions can be made:

1. The order $L1_0$ structure of the τ-MnAl phase could not be formed during the milling and annealing process in the Mn-Al system. By performing the milling process, Al atoms

dissolved in the Mn network and a single-phase β-Mn supersaturated solid solution was formed.

2. The formed β-Mn (SSSS) was unstable and transformed into the icosahedral quasi-crystal phase during annealing at temperatures lower than 680°C.

3. The icosahedral phase was converted into the stable phases of Al_8Mn_5 and β-Mn during the annealing process at higher temperatures (above 680°C).

6

DECLARATIONS

The authors declare that they have no known competing financial interests or personal relationships that could have appeared to influence the work reported in this paper.

FUNDING

The author received no financial support for the research, authorship, and/or publication of this article.

DATA AVAILABILITY

The author confirms that the data supporting the findings of this study are available within the article [and/or] its supplementary materials.

REFERENCES

[1] Liu, Z.W., Chen, C., Zheng, Z.G., Tan, B.H., Ramanujan, R.V., "Phase transitions and hard magnetic properties for rapidly solidified MnAl alloys doped with C, B, and rare earth elements", Journal of Materials Science, 2012, 47, 2333-2338.

[2] Jiménez-Villacorta, F., Marion, J.L., JOldham, T., Daniil, M., Willard, M.A., Lewis, L.H., "Magnetism-structure correlations during the ε→τ transformation in rapidly-solidified MnAl nanostructured alloys", Metals, 2014, 4, 8-19.

[3] Jia, Y., Wua, Y., Zhao, S., Wang, J., Jiang, C., "Relation between solidification microstructure and coercivity in MnAl permanent-magnet alloys", Intermetallics, 2018, 96, 41-48.

[4] Singh, N., Mudgil, V., Anand, K., Srivastava, A.K., Kotnala, R.K., Dhar, A., "Influence of processing on structure property correlations in τ -MnAl rare-earth free permanent magnet material", Journal of Alloys and Compounds, 2015, 633, 401-407.

[5] Fang, H., Kontos, S., Ångström, J., Cedervall, J., Svedlindh, P., Gunnarsson, K., Sahlberg, M., "Directly obtained τ-phase MnAl, a high-performance magnetic material for permanent magnets", Journal of Solid State Chemistry, 2016, 237, 300-306.

[6] Park, J.H., Hong, Y.K., Bae, S., Lee, J.J., Jalli, J., Abo, G.S., Neveu, N., Kim, S.G., Choi, C.J., Lee, J.G., "Saturation magnetization and crystalline anisotropy calculations for MnAl permanent magnet", Journal of Applied Physics, 2010, 107, 09A731.

[7] Matsumoto, M., Morisako, A., Kohshiro, N., "Crystal structure and magnetic properties of Mn-Al-Ni ferromagnetic films", Journal on Magnetics in Japan, 1991, 6, 134-140.

[8] Zeng, Q., Bakera, I., Cui, J.B., Yan, Z.C., "Structural and magnetic properties of nanostructured Mn-Al-C magnetic materials", Journal of Magnetism and Magnetic Materials, 2007, 308, 214-226.

[9] Wang, H.X., Si, P.Z., Jiang, W., Lee, J.G., Choi, C.J., Liu, J.J., Wu, Q., Zhong, M., Ge, H.L., "Structural stabilizing effect of Zn substitution on MnAl and its magnetic properties", Journal of Microphysics, 2011, 1, 19-22.

[10] Manchanda, P., Kashyap, A., Shield, J.E., Lewis, L.H., Skomski, R., "Magnetic properties of Fe-doped MnAl", Journal of Magnetism and Magnetic Materials, 2014, 365, 88-92.

[11] Mix, T., Bittner, F., Müller, K.H., Schultz, L., Woodcock, T.G., "Alloying with a few atomic percent of Ga makes MnAl thermodynamically stable", Acta Materialia, 2017, 128, 160-165.

[12] Xiang, Z., Xu, C., Wang, T., Song, Y., Yang, H., Lu, W., "Enhanced magnetization and energy product in isotropic nanocrystalline $Mn_{55}Al_{45}$ alloys with boron doping", Intermetallics, 2018, 101, 13-17.

[13] Xiang, Z., Song, Y., Deng, B., Cui, E., Yu, L., Lu, W., "Enhanced formation and improved thermal stability of ferromagnetic τ phase in nanocrystalline $Mn_{55}Al_{45}$ alloys by Co addition", Journal of Alloys and Compounds, 2019, 783, 416-422.

[14] Xiang, Z., Deng, B., Zhang, X., Wang, X., Cui, E., Yu, L., Song, Y., Lu, W., "Nanocrystalline MnAlV rare-earth-free permanent magnetic alloys with improved magnetization and thermal stability", Intermetallics, 2020, 116, 1-6.

[15] Lucis, M.J., Prost, T.E., Jiang, X., Wang,

M., Shield, J.E., "Phase transitions in mechanically milled Mn-Al-C permanent magnets", Metals, 2014, 4, 130-140.

[16] Jian, H., Skokov, K.P., Gutfleisch, O., "Microstructure and magnetic properties of Mn-Al-C alloy powders prepared by ball milling", Journal of Alloys and Compounds, 2015, 622, 524-528.

[17] Lu, W., Niu, J., Wang, T., Xia, K., Xiang, Z., Song, Y., Zhang, H., Yoshimura, S., Saito, H., "Low-energy mechanically milled τ-phase MnAl alloys with high coercivity and magnetization", Journal of Alloys and Compounds, 2016, 675, 163-167.

[18] Law, J.Y., Rial, J., Villanueva, M., Lopez, N., Camarero, J., Marshall, L.G., Blazquez, J.S., Borrego, J.M., Franco, V., Conde, A., Lewis, L.H., Bollero, A., "Study of phases evolution in high-coercive MnAl powders obtained through short milling time of gas-atomized particles", Journal of Alloys and Compounds, 2017, 712, 373-378.

[19] Rial, J., Svec, P., Palmero, E.M., Camarero, "Severe tuning of permanent magnet properties in gas-atomized MnAl powder by controlled nanostructuring and phase transformation", Acta Materialia, 2018, 157, 42-52.

[20] Amini Rastabi, R., Ghasemi, A., Tavoosi, M., Sodaee, T., "Magnetic characterization of nanocrystalline $Fe_{80-x}Cr_xCo_{20}$ ($15 \leq x \leq 35$) alloys during milling and subsequent annealing", Journal of Magnetism and Magnetic Materials, 2016, 416, 174-178.

[21] Amini Rastabi, R., Ghasemi, A., Tavoosi, M., Ramazani, M., "Magnetic features of Fe-Cr-Co alloys with tailoring chromium content fabricated by spark plasma sintering", Journal of Magnetism and Magnetic Materials, 2017, 426, 744-749.

8